Formation of a Manganese Tricarbonyl on the MgO Surface from $Mn_2(CO)_{10}$: Characterization by Infrared, Electron Paramagnetic Resonance, and X-ray Absorption Spectroscopies†

Supattra Khabuanchalad,[‡,§] Jatuporn Wittayakun,*[,‡] Rodrigo J. Lobo-Lapidus,[§] Stefan Stoll,[||] R. David Britt,[||] and Bruce C. Gates*[,§]

School of Chemistry, Institute of Science, Suranaree University of Technology, Nakhon Ratchasima, Thailand, 30000, and Department of Chemical Engineering and Materials Science and Department of Chemistry, University of California, Davis, California 95616

Received: May 8, 2010; Revised Manuscript Received: August 17, 2010

The goal of this work was to prepare structurally well-defined manganese complexes on high-area MgO powder by vapor deposition of $Mn_2(CO)_{10}$. The supported species were characterized by infrared (IR), electron paramagnetic resonance (EPR), and X-ray absorption spectroscopies. The results show that when the manganese loading of the sample was 3.0 wt %, most of the $Mn_2(CO)_{10}$ was physisorbed, but when the loadings were less, chemisorbed species predominated, being formed by adsorption of $Mn_2(CO)_{10}$ on hydroxyl groups on the MgO surface. Treatment of samples containing 1.0 wt % Mn with O_2 at room temperature resulted in oxidation of the manganese and the formation of surface species that are well represented as the d^4 complex $Mn(CO)_3(O_s)_3$ (where O_s is surface oxygen of MgO), as indicated by IR and extended X-ray absorption fine structure (EXAFS) spectra. The EXAFS data show Mn−C, C≡O, and Mn−O_s bond lengths as 1.90, 1.43, and 1.98 Å, respectively.

Introduction

Oxide-supported metal complexes are widely investigated materials that find important applications as industrial catalysts.[1,2] They offer unique opportunities for fundamental investigations of organometallic compounds in the absence of solvents, because they may be understood as metal complexes incorporating extremely heavy ligands—the supports—allowing investigation of their chemistry in the presence of gas-phase reactants.

The supports in supported metal complex catalysts are typically porous metal oxides,[3] chosen because they provide high surface areas on which the metal complexes can be highly dispersed—giving high catalytic activities per unit volume of material. Some of the best understood supported metal complexes are carbonyls of group 8 metals.[4] The chemistry of carbonyls of group 7 metals has also been investigated, for example, that of rhenium carbonyls, including mono-, di-, and trinuclear species,[5,6] but only little has been reported about supported complexes of manganese.

Here we report an investigation of samples prepared by the reaction of dimanganese decacarbonyl, $Mn_2(CO)_{10}$, with MgO and reactions of the supported species. Manganese was chosen because its complexes are important in homogeneous catalysis,[7,8] and their supported analogues might be expected to be good candidate catalysts, being characterized by robustness and ease of separation from products combined with the uniformity and selectivity of homogeneous catalysts. $Mn_2(CO)_{10}$ was chosen as the precursor because it is reactive with metal oxides and zeolites (e.g., γ-Al_2O_3,[9] MCM-41,[10] and zeolite NaY[11]), and the infrared (IR) spectra of CO ligands on the resulting surface species provide valuable information about the structure and bonding of the metal complexes. The high vapor pressure of $Mn_2(CO)_{10}$ allows sample preparation by chemical vapor deposition (CVD).

MgO was chosen as a support because it is available as a powder with high surface area, facilitating the preparation of surface species in samples with high enough loadings of the metal complex per unit volume to give good signal-to-noise ratios in the spectra.[12,13]

Our specific goal was to elucidate the surface chemistry of relatively well defined manganese carbonyls on MgO by taking advantage of a set of methods that are highly complementary and expected to provide insight into the structures of the surface species, namely, IR, electron paramagnetic resonance (EPR), extended X-ray absorption fine structure (EXAFS), and X-ray absorption near edge structure (XANES) spectroscopies.

Experimental Methods

Treatment of MgO. MgO powder (EMD Science, 98.0%) was calcined in flowing dry O_2 (Airgas, 99.9999%) as the temperature was ramped from room temperature to 673 K at a rate of 3 K/min, then held in flowing O_2 at 673 K for 4 h, and subsequently treated under vacuum (pressure $\approx 1 \times 10^{-3}$ mbar) at 673 K for an additional 16 h. The calcined MgO, which had been partially decarbonated and partially dehydroxylated, was kept under vacuum as it was cooled to room temperature, and then it was stored in an N_2-filled glovebox (Vacuum Atmospheres, with O_2 and moisture contents each <1.0 ppm) before being used for the preparation of the supported manganese complexes or subjected to characterization by IR and EPR spectroscopies (as described below). The BET surface area of the calcined MgO was approximately 70 m^2/g.

† Part of the "D. Wayne Goodman Festschrift".

* To whom correspondence should be addressed. E-mail: jatuporn@sut.ac.th (J.W.); bcgates@ucdavis.edu (B.C.G.).

‡ Suranaree University of Technology.

§ Department of Chemical Engineering and Materials Science, University of California.

|| Department of Chemistry, University of California.

10.1021/jp104205q
Published on Web 09/17/2010

Synthesis of MgO-Supported Samples from $Mn_2(CO)_{10}$. The MgO-supported samples were synthesized from $Mn_2(CO)_{10}$ (Strem, 98.0%). The synthesis and handling were performed with exclusion of air and moisture on a double-manifold Schlenk line. Glassware was dried at 393 K overnight prior to use. In an N_2-filled glovebox, a flask containing the highly volatile $Mn_2(CO)_{10}$ was quickly connected to another flask containing calcined MgO powder via a glass tube equipped with a Teflon valve separating the two flasks and ground-glass joints. The apparatus was removed from the glovebox and connected to the Schlenk line via a line with a Teflon valve. The flask containing $Mn_2(CO)_{10}$ was placed in a dry ice/2-propanol bath (temperature $\approx$ 248 K). The system was evacuated for 15 min and then warmed to room temperature in static vacuum to allow sublimation of the $Mn_2(CO)_{10}$. The masses of $Mn_2(CO)_{10}$ and MgO were chosen to give supported samples containing 0.10, 1.0, and 3.0 wt % Mn. Each sample was evacuated overnight and stored in the glovebox.

Sample Treatment. ***Decarbonylation in the Presence of H_2.*** The samples formed from $Mn_2(CO)_{10}$ on MgO were decarbonylated in the presence of flowing H_2 in a once-through quartz tubular flow reactor. The powder sample (0.50 g) was loaded into the reactor in the glovebox. The sample was held by a frit mounted near the center of the tube, which was sealed on both ends with O-ring compression fittings. The tube was removed from the glovebox and held in an electrically heated tube furnace, and then both ends of the reactor were connected to the flow system, all without exposure of the sample to air. The temperature in the reactor was measured below the frit with a K-type thermocouple. H_2 (Airgas, 99.9999%) flowed through the reactor at 70 mL(NTP)/min as the temperature was ramped to 973 K at a rate of 2 K/min. The temperature of the reactor was held at 973 K for 2 h, and then it was cooled to room temperature while the H_2 flow continued. The effluent gases from the reactor were analyzed by an online mass spectrometer (Pfeiffer Vacuum, OmniStar). The reactor was then flushed with helium (Praxair, 99.999%) before being transferred back to the glovebox.

Treatment in O_2. Each sample was loaded into a once-through quartz tubular flow reactor and connected to the flow system as in the decarbonylation experiment. At room temperature, O_2 (Airgas, 10% by volume in helium) was fed to the reactor at 60 mL(NTP)/min for 6 h, then the sample was flushed with helium, and the reactor was sealed and returned to the glovebox. In some experiments, the effluent was analyzed with the online mass spectrometer.

Sample Characterization. ***IR Spectroscopy.*** The MgO support and the supported samples were characterized by IR spectroscopy at room temperature with a Bruker IFS 66v Fourier transform spectrometer equipped with DTGS and HgCdTe detectors. In the glovebox, each sample was pressed between two KBr windows and placed in a gastight cell (International Crystal Laboratories). The cell was then loaded into an airtight container as a precaution to minimize air exposure before transfer of the cell to the spectrometer. The sample chamber of the spectrometer was evacuated (pressure $\approx$ 1 mbar), and the vacuum was maintained as spectra of the sample were recorded in transmission mode with a resolution of 4 cm^{-1}. Each reported spectrum is the average of 128 scans.

EPR Spectroscopy. The untreated and calcined MgO and the supported samples prepared from $Mn_2(CO)_{10}$ were characterized by EPR spectroscopy. Each sample in the N_2-filled glovebox was loaded into a 4 mm o.d. quartz EPR tube and sealed with an Ultra-torr fitting. The EPR tube was removed from the glovebox and evacuated (pressure $\approx 1 \times 10^{-3}$ mbar) for 30 min and then flame-sealed. EPR data were collected at the CalEPR center at the University of California, Davis. Each sample was scanned at room temperature in a Bruker ECS 106 X-band ($\approx$9.5 GHz) spectrometer equipped with a Bruker ER4102ST cavity operating in the TE_{102} mode. Measurements were performed with a microwave power of 10 mW, a field modulation of 0.2 mT at 100 kHz, and a sweep rate of 0.1 mT/s. For each spectrum, 10 scans were accumulated.

EXAFS Spectroscopy. The sample formed from $Mn_2(CO)_{10}$ and MgO (1.0 wt % Mn) after treatment in O_2 was characterized by X-ray absorption spectroscopy. Data collection was performed at beamline 9-BM at the Advanced Photon Source (APS) at Argonne National Laboratory. The beamline is equipped with a double-crystal Si(111) monochromator which was detuned by approximately 30% at the Mn K edge to minimize the presence of higher harmonics in the X-ray beam. The intensity of the X-rays entering and exiting the sample was measured with two gas-filled ion chambers (FMB-Oxford), and a third ion chamber was used to collect the spectrum of a manganese foil used as a reference for energy calibration.

The sample was loaded into a stainless steel vacuum tube sealed with O-rings and transferred to the synchrotron, where it was handled in an N_2-filled glovebox; the O_2 and moisture contents of the glovebox were 0.10 and 1.3 ppm, respectively. The mass of the sample was calculated to provide an absorbance of about 2.5 and an optimized signal-to-noise ratio. The sample was weighed, mixed with inert boron nitride powder (Aldrich, 98.0%, particle diameter $\cong$ 1 μm), pressed into a self-supporting wafer, and loaded into the cell,[14] which allowed scanning of the sample without exposure to air. The cell was transferred to the beamline and mounted between the first two ion chambers. The sample was scanned at room temperature in transmission mode at the Mn K edge (6539 eV) with a step size of 0.07k (k is the wave vector) in the EXAFS region. The reported spectrum is the average of five spectra.

EXAFS Data Analysis. EXAFS data analysis was conducted by using the "difference file" technique[15] with the software XDAP.[16] First, the five scans were aligned and averaged. The functions used to construct the structural models and minimize the error are shown elsewhere.[15] Reference backscattering amplitudes were calculated by use of the FEFF7.0[17] software. Crystallographic data characterizing $Mn_2(CO)_{10}$[18] for the representation of Mn−C, Mn−O* (O* is carbonyl oxygen; the Mn−C−O moiety is characterized by collinear multiple scattering), and Mn−Mn contributions were included in the fitting. Crystallographic data characterizing Mn_2O_3 and MnMg alloy[19] were used for Mn−O_s (Mn−O_s refers to a relatively short Mn−O distance in supported samples incorporating oxygen of the support surface) and Mn−Mg contributions, respectively.

The fitting was done in R-space (distance space) by using three k-weightings (k^0, k^1, and k^2). In the fitting with a candidate model, the parameters characterizing each contribution, the coordination number N, the $\Delta\sigma^2$ value (Debye−Waller factor), the interatomic distance R, and the inner potential correction ΔE_0 were varied until an optimized fit was obtained for all k-weightings. For a candidate model to be considered acceptable, it was required to fit satisfactorily with all the k-weightings. The EXAFS data were analyzed with 11 free parameters over the range $3.08 < k < 9.50$ $Å^{-1}$. The number of parameters used in the fitting did not exceed the statistically justified number calculated with the Nyquist theorem[20] (14.3).

Two criteria were used to determine whether an EXAFS fit was satisfactory: First, analysis was done to determine whether

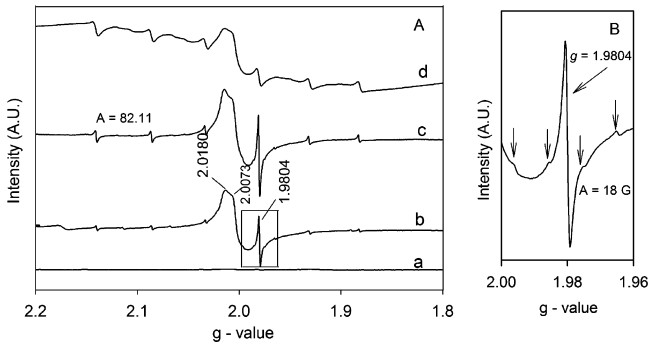

Figure 1. (A) EPR spectra of untreated MgO (a), MgO after treatment in O_2 at 673 K followed by evacuation at the same temperature (b), sample prepared from $Mn_2(CO)_{10}$ on MgO (0.10 wt % Mn) (c), and sample prepared from $Mn_2(CO)_{10}$ on MgO (1.0 wt % Mn) (d); (B) magnification of part A, spectrum b, at $g \approx 1.9804$.

the addition of each shell to the model decreased the value of $(\Delta\chi)^2$.[21] Second, the parameters for each shell were checked to determine whether they were physically appropriate; specifically, the value of ΔE_0 was considered to be appropriate in the range -10 to 10 eV and the value of $\Delta\sigma^2$ was constrained not to exceed 1.5×10^{-2} Å^{-2}.

XANES Data Analysis. Data in the XANES region were analyzed with the software Athena.[22] The edge position of the manganese in the sample was taken as the inflection point in the measured X-ray absorption spectrum. The energy scale of the XAFS spectrum was calibrated by setting the edge position of the manganese foil to the reported value. The reported XANES spectrum is the average of five spectra.

Results

Spectroscopic Characterization of MgO. The EPR spectrum of MgO calcined at 673 K (Figure 1A, spectrum b) lacks information that would identify the MgO, but the data provide evidence of impurities in the MgO. The spectrum includes signals at $g = 2.0073$ and 2.0180 which match reported signals of the carbonate radical, CO_3^-.[23,24] The signal at $g = 1.9804$, including a very weak quartet (coupling constant $A = 18$ G) (Figure 1B), matches the g value of chromium, reported at $g = 1.9804$.[25] The quartet corresponds to ^{53}Cr (the natural abundance of this isotope is 9.3%), which has a nuclear spin I of 3/2. A weak sextet of hyperfine lines with a coupling constant of 82.11 G attributed to Mn^{2+} species ($I = 5/2$) was also observed in this sample. These impurities are common in commercial MgO samples.[26] The signal corresponding to oxygen radicals was not observed in the spectrum of this sample.

Evidence of the surface chemistry of the MgO is provided by the IR spectra. The spectrum of the calcined MgO (Figure 2D) includes bands in the interval between 3725 and 3775 cm^{-1}, which are assigned on the basis of results reported by Diwald et al.[27] The high-frequency (3767 cm^{-1}) component is assigned to OH groups in which the oxygen atom bonds to one surface cation (one-coordinated OH group), whereas the low-frequency component is assigned to OH groups in which the oxygen atom is coordinated with three to five cations (three-, four-, and five-coordinated OH groups).

The carbonate region of the IR spectrum characterizing the calcined MgO (Figure 3A) shows the presence of peaks at 1484 and 1422 (cm^{-1}), which are assigned to monodentate carbonate and carboxylate group, respectively.[28]

Reaction of $Mn_2(CO)_{10}$ with Partially Dehydroxylated MgO. ***Observations During Synthesis.*** As the yellow-colored $Mn_2(CO)_{10}$ was deposited onto MgO powder from the vapor phase, the color of the powder changed from white to pale yellow, indicating that the precursor had been adsorbed. The sample remained pale yellow after subsequent overnight evacuation.

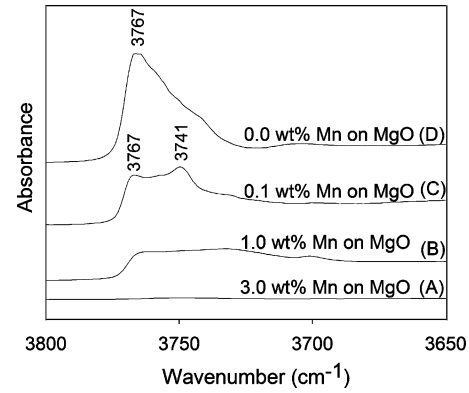

Figure 2. Normalized IR spectra in the ν_{OH} region characterizing sample prepared from $Mn_2(CO)_{10}$ on MgO. The respective Mn contents (wt %) of the samples were 3.0 (A), 1.0 (B), 0.10 (C), and 0.0 (D). Spectra were normalized with respect to the carbonate band at 1264 cm^{-1}.

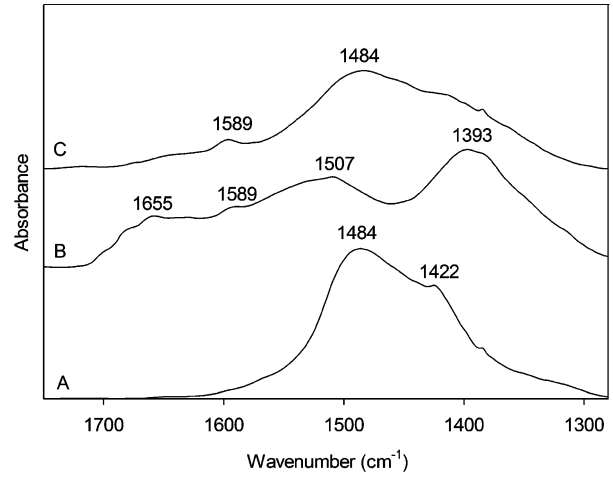

Figure 3. Normalized IR spectra in the carbonate region characterizing MgO (A), sample prepared from $Mn_2(CO)_{10}$ on MgO (1.0 wt % Mn) (B), and after treatment in O_2 (C). The spectra were normalized by setting the value of the intensity of the strongest band in each spectrum equal to 1.0.

IR Evidence of Reactions of $Mn_2(CO)_{10}$ with Surface OH Groups of MgO. When the manganese loading of the sample was only 0.10 wt %, the intensity of the band characteristic of the singly coordinated OH group (at 3767 cm^{-1}) decreased after the $Mn_2(CO)_{10}$ had been adsorbed, but the intensity of the band at approximately 3741 cm^{-1} remained essentially unchanged (Figure 2C). These results indicate that adsorption of $Mn_2(CO)_{10}$ on MgO took place initially on the singly coordinated OH groups. The spectrum shows that this low loading of manganese was not sufficient to convert all the surface hydroxyl groups.

When the loading of manganese on the MgO was increased to 1.0 and then to 3.0 wt %, the intensities of both hydroxyl bands decreased, and they finally became unobservable (Figure 2, spectra B and A, respectively). Thus, when the manganese loading was 3.0 wt %, all the hydroxyl groups had reacted, and some of the precursor might have interacted with sites other than OH groups on the MgO.

IR Evidence of Reactions of $Mn_2(CO)_{10}$ with Surface CO_3^{2-} Groups of MgO. When $Mn_2(CO)_{10}$ was adsorbed on MgO, there was a decrease in intensity of the IR band at 1484 cm^{-1} (Figure

TABLE 1: ν_{CO} IR Bands Characterizing Isolated and Supported Manganese Carbonyl Complexes

sample (comment)	metal coordn no.	no. of Mn valence electrons	ν_{CO} band position (cm^{-1})	no. of ν_{CO} bands	ref
$Mn_2(CO)_{10}$ in CH_2Cl_2	6	18	2045(m), 2011(s), 1979(w)	3	this work
sample formed from $Mn_2(CO)_{10}$ on MgO and containing 0.1 wt % Mn (and represented as $Mn(CO)_3(O_s)_3$)[a]	N.A.	N.A.	2029 (s), 1934(s), 1895(m)	3	this work
sample formed from $Mn_2(CO)_{10}$ on MgO and containing 1.0 wt % Mn	N.A.	N.A.	2038(m), 1937(s), 1895(s)	3	this work
sample formed from $Mn_2(CO)_{10}$ on MgO and containing 1.0 wt % Mn after O_2 treatment	3	16	2042(s), 1947(s), 1905(s)	3	this work
$[Mn(CO)_5]^-$ on MgO (inferred to be weakly interacting with surface)	5	18	1891, 1863	2	29
$[Mn(CO)_5]^-$ on MgO (inferred to be ion paired with Mg^{2+} sites)	5	18	2035, 1916, 1898, 1800	4	29
$Mn(CO)_5H$ in THF solution	6	18	2118 (vw), 2016(vs), 2007(s)	3	29
$[Mn(CO)_5]^-$ in THF solution	5	18	1898, 1863	2	29
$CH_3Mn(CO)_5$	6	18	2045(sh), 2023.6(vs), 2002(s,sh), 1961(w,sh)	4	30
$[Mn(CO)_5\{C(O)O(C_7H_{15})\}]$	6	18	2124(w), 2031(s), 2007(s)	3	31
$[Mn(CO)_3(tripod)]^+$ [b]	6	18	2030(s), 1962(s), 1902(ms), 1860(s)	4	29
$[Mn(CO)_3(PEt_3)_3^+][ClO_4^-]$ in CH_2Cl_2 solution	6	18	2021(s), 1943(s)	2	32
$Mn(CO)_3(triphos)^+$ [c]	6	18	2026(s), 1960(sh), 1945(s)	3	32
mer,*trans*-$[MnBr(CO)_3\{P(C_6H_4Cl\text{-}4)_3\}_2]$	6	18	2033(w), 1951(vs), 1901(s)	3	33
mer,*trans*-$[MnBr(CO)_3P(CH_2C_6H_4)_3\}_2]$	6	18	2031(w), 1945(vs), 1912(s)	3	33
mer,*trans*-$[MnBr(CO)_3\{P(C_6H_4OMe\text{-}4)_3\}_2]$	6	18	2031(w), 1946(vs), 1908(s)	3	33
fac,*cis*-$[MnBr(CO)_3(dppb)]$[d]	6	18	2028(s), 1962(s), 1910(s)	3	33
$[Mn(CO)_3(3,5\text{-}DBCat)]^-$ [e] in CH_2Cl_2 solution	5	16	1998(s), 1891(br)	2	34
$[Mn(CO)_3(3,5\text{-}DBCat)]^-$ [e] in CH_2Cl_2 solution at 193 K	5	16	1998(s), 1894(s), 1883(s)	3	34
$[Mn(CO)_3(3,5\text{-}DBCat)(py)]^-$ [f] in pyridine solution	6	18	1995(s), 1885(s), 1862(s)	3	34
$[Mn(CO)_3(3,5\text{-}DBCat)(PPh_3)]^-$ [g] in CH_2Cl_2 solution	6	18	2001(s), 1904(s), 1867(s)	3	34
$[Mn(CO)_3(S,S\text{-}C_6H_4)]^-$ in THF solution	5	16	1996(vs), 1887(s)	2	35
$[Mn(CO)_3(S\text{-}C_5H_4\text{-}N)(S\text{-}C_5H_4N)]^-$ in THF solution	6	18	1994(vs), 1901(s), 1801(s)	3	35
$[Mn(CO)_3(H_2O)_3]^+$	6	18	2051, 1944	2	36
fac-$MnBr(CO)_3[H(pzAn^{Me})]$[h] (a manganese tricarbonyl with 3 nitrogen-containing ligands)	6	18	KBr: 2029, 1923, 1902	3	37
$\{fac\text{-}Mn(CH_3CN)(CO)_3[H(pzAn^{Me})]\}^h$ (PF_6) (a manganese tricarbonyl with 3 nitrogen-containing ligands)	6	19	KBr: 2052, 1956, 1919	3	37
$[fac\text{-}Mn(CO)_3(l\text{-}pzAn^{Me})]_2$[h] (a manganese tricarbonyl with 3 nitrogen-containing ligands)	6	19	KBr: 2002, 1905, 1884	3	37
$(n\text{-}Bu_4N)_2[Mn(CO)_3(H_2O)\{Mo_5O_{13}(OMe)_4(NO)\}]$ (a manganese tricarbonyl with 3 oxygen-containing ligands)	6	18	2029(s), 1933(s), 1916(s)	3	47
$(n\text{-}Bu_4N)_3[Na\{Mo_5O_{13}(OMe)_4(NO)\}_2\{Mn(CO)_3\}_2]\cdot MeOH$ (a manganese tricarbonyl with 3 oxygen-containing ligands)]	6	18	2036(s), 1930(s), 1920(s),	3	47
$Mn(CO)_3(C_5H_5)Co\{P(O)R_2\}_3$	6	N.A.	2033, 1920	2	48
$Re_2(CO)_{10}$ in cyclohexane solution	6	18	2070, 2014, 1976	3	49
$Re(CO)_3\{O\text{-}Mg\}\{OH\text{-}Mg\}_2$	6	N.A.	2028, 1905, 1862	3	50

[a] O_s = oxygen originating from the support. [b] tripod = 1,1,1-tris((diphenylphosphino)methyl)ethane. [c] triphos = bis(2-(diphenylphosphino)ethyl)phenylphosphine. [d] dppb = 1,4-bis(diphenylphosphino)butane. [e] 3,5-DBCat = 3,5-di-*tert*-butylcatecholate. [f] py = pyridine. [g] PPh_3 = triphenylphosphine. [h] $H(pzAn^{Me})$ = 2-(pyrazolyl)-4-toluidine ligand.

3A,B) assigned to monodentate carbonate[28] on MgO, and there was an increase in intensity of a band at 1393 cm^{-1}, assigned to carboxylates, relative to those at 1484 and 1422 cm^{-1}, which are not visible in the spectrum after adsorption.[28] This result indicates that the $Mn_2(CO)_{10}$ interacts weakly with the carbonate groups on MgO upon adsorption.

Characterization of Sample Containing 3.0 wt % Mn. ***IR Spectra.*** The interpretation of the IR spectra of the highly loaded sample is based on a comparison of the observed IR bands with those reported for a family of manganese carbonyl compounds, including $Mn_2(CO)_{10}$ (Table 1). The spectrum characterizing the sample containing 3.0 wt % Mn includes two broad, intense bands, at 2050(m) and 2011(s) cm^{-1} (Figure 4C). These bands essentially match those characterizing $Mn_2(CO)_{10}$ in CH_2Cl_2 solution (Table 1 and Figure 4D). Furthermore, the spectrum also includes a shoulder at approximately 2029 cm^{-1} and a broad absorption extending from approximately 1889 to 1981 cm^{-1}. The similarity of the two intense bands to those in the spectrum of the precursor indicates that some of the $Mn_2(CO)_{10}$ was adsorbed on MgO with its structure essentially intact; the data do not determine the degree of any aggregation of the $Mn_2(CO)_{10}$ on the surface (thus, they do not determine whether it was molecularly dispersed). The broad lower-frequency absorption suggests the presence of adsorbed species other than $Mn_2(CO)_{10}$,

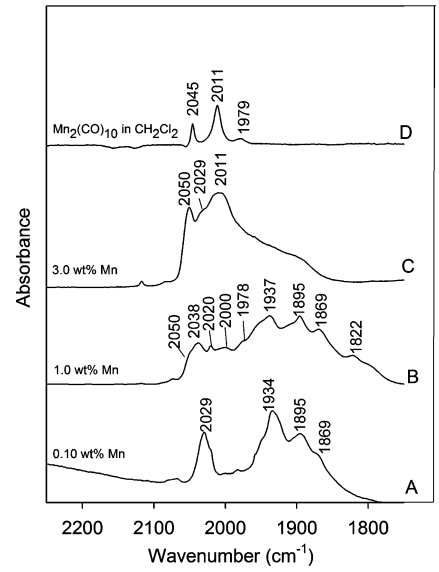

Figure 4. Normalized IR spectra in the ν_{CO} region characterizing a sample prepared from $Mn_2(CO)_{10}$ on MgO. The respective Mn contents (wt %) of the samples were 0.10 (A), 1.0 (B), and 3.0 (C). Spectra A−C were normalized with respect to the carbonate band at 1264 cm^{-1}. Spectrum D corresponds to $Mn_2(CO)_{10}$ in CH_2Cl_2 solution.

and our goal in investigating samples with lower loadings of $Mn_2(CO)_{10}$ was to characterize these latter adsorbed species.

Characterization of Sample Containing 0.10 wt % Mn. ***IR Spectra.*** The IR spectrum of the sample with the lowest manganese loading (0.10 wt %) (Figure 4A) was markedly different from that of the sample with the high loading (and different from that of $Mn_2(CO)_{10}$). The spectrum includes three intense bands, at 2029(m), 1934(s), and 1895(m) cm^{-1}, which fall in the range reported for a number of manganese tricarbonyl compounds (Table 1).[29−37] The data characterizing these manganese carbonyl compounds (Table 1) show that the positions of the carbonyl bands depend on the non-carbonyl ligands on the manganese. We therefore hypothesize that the adsorption of $Mn_2(CO)_{10}$ took place by a reaction with hydroxyl groups of MgO that formed manganese tricarbonyls with the support as a ligand.

Furthermore, the spectrum of the sample containing 0.10 wt % Mn (Figure 4A) includes a weak shoulder at about 1869 cm^{-1}. By comparison with the spectra of manganese pentacarbonyls (Table 1), we might suggest that the shoulder indicates the presence of manganese pentacarbonyls on the MgO surface. Manganese pentacarbonyls typically are characterized by a band at about 1898 cm^{-1}; however, any peaks with frequencies near this would likely overlap bands of the manganese tricarbonyl species, and therefore we are not able to draw a conclusion about the presence of manganese pentacarbonyls on the surface from this region of the spectra.

EPR Spectroscopy. The EPR spectrum of the sample containing 0.10 wt % Mn (Figure 1A, spectrum c) includes a signal at $g = 2.0015$ and a sextet of hyperfine lines with a coupling constant 82.11 G, which is characteristic of isolated Mn^{2+}.[38] The spectrum of this sample also includes signals at $g = 2.0180$ and $g = 2.0073$, which correspond to CO_3^- on MgO, which indicates that the decarbonation during the calcination was not complete. Furthermore, the signal characteristic of the chromium impurity in the MgO was still observed.

The presence of the Mn^{2+} signal demonstrates that the manganese was oxidized as it reacted with the MgO (the manganese in $Mn_2(CO)_{10}$ is formally Mn^0), consistent with our IR evidence that $Mn_2(CO)_{10}$ reacted with the MgO. We emphasize that this evidence of Mn^{2+} does not rule out the presence of manganese in other oxidation states that are not EPR active.

Characterization of Sample Containing 1.0 wt % Mn. ***IR Spectroscopy.*** The IR spectrum characterizing the sample prepared from $Mn_2(CO)_{10}$ on MgO containing 1.0 wt % Mn (Figure 4B) includes bands in the ν_{CO} stretching region, at 1822, 1869, 1895, 1937, 1978, 2000, 2020, 2038, and 2050 cm^{-1}. The locations of these bands differ from those of the bands characterizing $Mn_2(CO)_{10}$ and the supported samples incorporating 0.10 and 3.0 wt % Mn. These IR bands are assigned to manganese carbonyl species, as follows: the bands at 2038(m), 1937(s), and 1895(s) cm^{-1} are in the range of those reported for manganese tricarbonyl compounds, as summarized in Table 1. The band at 1869 cm^{-1} is characteristic of manganese pentacarbonyl compounds (Table 1). The small peak at about 1822 cm^{-1} could also correspond to a manganese pentacarbonyl, and some of the bands (at 2050, 2000, and 1978 cm^{-1}) correspond to $Mn_2(CO)_{10}$ itself. Thus, we infer from the IR spectra that the sample prepared from $Mn_2(CO)_{10}$ that contained 1.0 wt % Mn included a mixture of at least these three manganese carbonyl species, including unreacted precursor.

EPR Spectroscopy. The EPR spectrum characterizing the sample containing 1.0 wt % Mn (Figure 1A, spectrum d)

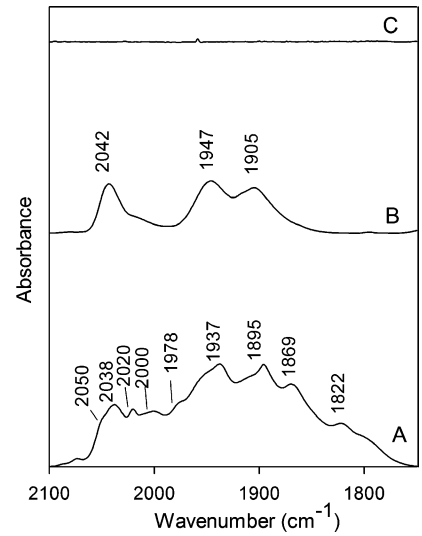

Figure 5. Normalized IR spectra in the ν_{CO} region of sample prepared from $Mn_2(CO)_{10}$ and MgO (1.0 wt % Mn) (A), sample from spectrum A after treatment in flowing O_2 (B), and sample from spectrum A after decarbonylation (C).

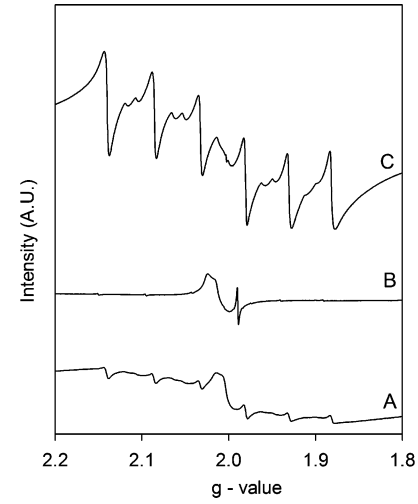

Figure 6. EPR spectra of sample prepared from $Mn_2(CO)_{10}$ and MgO (1.0 wt % Mn) (A), sample of spectrum A after treatment in flowing O_2 (B), and sample of spectrum A after decarbonylation (C).

includes the sextet of hyperfine lines mentioned above (coupling constant = 82.11 G) that is characteristic of Mn^{2+},[38] along with signals at $g = 2.0180$ and $g = 2.0073$ corresponding to the CO_3^- radical and the signal at $g = 1.9804$ characterizing the chromium impurity. Moreover, a broad baseline was observed, which results from dipolar interactions.[38] The presence of the baseline in the spectrum suggests that the distance between Mn atoms in the sample containing 1.0 wt % Mn was significantly less on average than that in the sample containing 0.1 wt % Mn.

Characterization of Sample Containing 1.0 wt % Mn Following Treatment in H_2. ***IR Spectra.*** The IR spectrum of the sample after treatment in flowing H_2 as the temperature was ramped to 973 K lacked bands in the ν_{CO} region (Figure 5C), indicating that all the carbonyl ligands had been removed.

EPR Spectra. The EPR spectrum of this decarbonylated sample (Figure 6C) is characterized by an intense sextet of hyperfine lines characteristic of Mn^{2+} species, with the intensity being greater than that characterizing the sample prior to treatment in H_2; evidently the treatment that led to decarbonylation of the manganese species affected the EPR signals, but

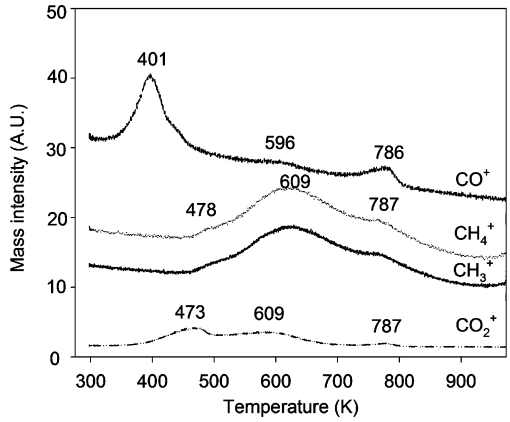

Figure 7. Mass spectra of effluent gases formed by treatment of samples prepared from $Mn_2(CO)_{10}$ on MgO (1.0 wt % Mn) in flowing H_2. The data are not normalized.

the data do not determine the ligands replacing CO on the manganese and, as discussed below, they do not simply indicate a change in the amount of Mn^{2+} in the sample.

Mass Spectra of Effluent Gas. As the sample was being treated in flowing H_2, mass spectra of the effluent gas were recorded (Figure 7). Consistent with the IR data demonstrating decarbonylation, the mass spectra of the effluent gas indicate the presence of CO in the effluent stream; furthermore, the effluent contained CO_2, CH_4, and CH_3 fragments presumably formed from CO, H_2, and possibly the support surface. As the temperature was ramped up, CO signals appeared at 401, 596, and 786 K, suggesting the presence of multiple surface manganese carbonyl species in the sample prior to treatment in H_2. The CO_2 signals appeared at temperatures higher than those characteristic of the CO, namely, at 473, 609, and 787 K, consistent with the formation of CO_2 by reaction of CO. Furthermore, the signals representing CH_4 and CH_3 were observed at 478, 609, and 787 K, suggesting that they were also formed in reactions of CO and H_2.

Characterization of Sample Containing 1.0 wt % Mn Following Treatment in O_2. ***IR Spectra in the ν_{CO} Region.*** The sample containing 1.0 wt % Mn was treated in flowing O_2 at room temperature. The sample color changed from pale yellow to light brown after the treatment. The IR spectrum changed as a result of the treatment (Figure 5A,B). The bands representing the untreated sample corresponding to $Mn_2(CO)_{10}$ on MgO (at 2050(sh), 2000(m), and 1978(sh) cm^{-1}) and that corresponding to manganese pentacarbonyls (at 1869(m) cm^{-1}) were no longer observed; we infer that these species were removed in the oxidative treatment. The resultant spectrum (Figure 5B) includes only three bands in the ν_{CO} region (at 2042(s), 1947(s), and 1905(s) cm^{-1}), which are in agreement with ν_{CO} bands characteristic of manganese tricarbonyls (Table 1). These three bands shifted slightly to higher frequencies as a result of the O_2 treatment. The IR spectrum of this O_2-treated sample was simpler than that of the initial sample, suggesting the presence of more nearly uniform surface species; consequently, we characterized this sample by EXAFS spectroscopy.

Mass Spectrum of Effluent Gas. The mass spectrum characterizing the effluent gas during the O_2 treatment (Figure 8) indicates the presence of CO, demonstrating that carbonyl ligands in the sample were removed during the O_2 treatment.

IR Spectra in Carbonate Region. The IR spectrum in the carbonate region representing the sample after the O_2 treatment (Figure 3C) shows an increase in the intensity of the band associated with monodentate carbonate (at 1484 cm^{-1}). This

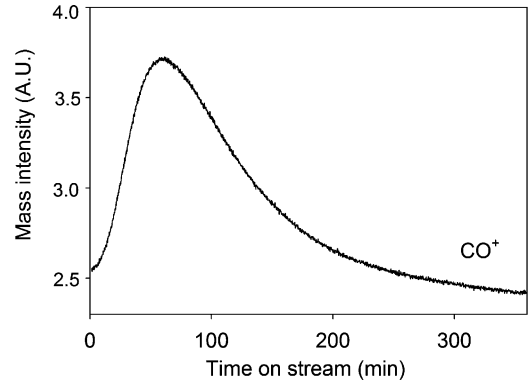

Figure 8. Mass spectra: CO^+ signal characterizing the effluent gas formed by treatment of samples prepared from $Mn_2(CO)_{10}$ on MgO (1.0 wt % Mn) in flowing O_2 at room temperature.

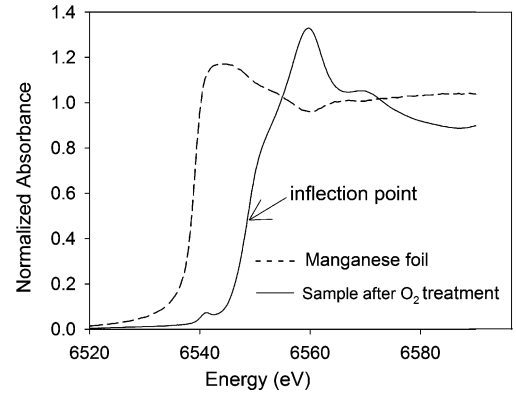

Figure 9. XANES spectra characterizing the sample prepared from $Mn_2(CO)_{10}$ on MgO (1.0 wt % Mn) after O_2 treatment and manganese foil.

result suggests that the O_2 treatment caused the formation of carbonate. Because the CO ligands attached to the Mn atoms were the only carbon-containing species in the sample, we infer that some of the CO was removed and reacted with O_2 and formed carbonate groups adsorbed on the MgO. This inference is supported by the evidence of removal of CO during the treatment as observed by the mass spectra of the effluent.

EPR Spectra. The signal of sextet hyperfine lines corresponding to Mn^{2+} was still observed in the spectrum of the sample after the O_2 treatment (Figure 6B), but its intensity was greatly reduced relative to that of the untreated sample (Figure 6A), indicating that almost all of the Mn^{2+} had been converted; we infer that the manganese had been oxidized. Furthermore, the broad baseline observed in the spectrum of the untreated sample was removed by the treatment, consistent with the inference that almost all the Mn^{2+} had been oxidized. These data are consistent with the IR spectra showing that the $Mn_2(CO)_{10}$ and manganese pentacarbonyl species were converted by reaction with O_2.

XANES Spectra. The XANES spectrum characterizing the sample containing 1.0 wt % Mn after treatment in O_2 is shown in Figure 9. The spectrum shows a significant shift in the edge position (relative to that of metallic manganese) to higher energies, strongly suggesting that the manganese in the sample was cationic, in agreement with the EPR results and the treatment conditions. The edge shift of 9.7 eV is compared with the literature values determined by XANES of various manganese compounds, shown in Figure 10. The comparison provides a basis for estimating the oxidation state of manganese in the O_2-treated sample, but the comparison is open to question because of the inconsistency of the literature values of the edge

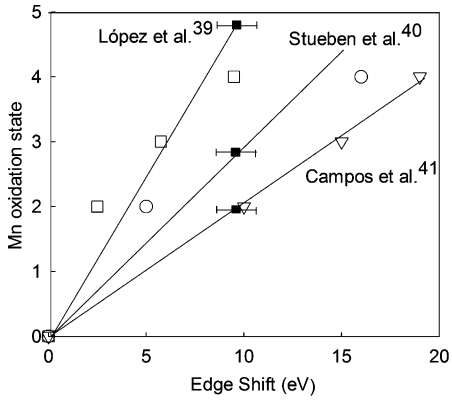

Figure 10. XANES calibration data and comparison with edge shift of supported manganese carbonyl species after treatment in O_2. Literature data characterizing standard samples (including manganese foil and manganese oxides) as shown: □, López et al.; ○, Stueben et al.; ▽, Campos et al.; ■, datum obtained in this work shown on each of the three lines to indicate the manganese oxidation state according to each of the three literature data sets.

energies. A comparison of our data with those of López et al.[39] (Figure 10) indicates manganese in an oxidation state of approximately +5, whereas a comparison of our data with those of Stueben et al.[40] indicates manganese in an oxidation state of approximately +3, and a comparison of our data with those of Campos et al.[41] indicates manganese in an oxidation state of approximately +2 (Figure 10). We discount the third of these possibilities on the basis of our EPR data indicating that almost all the Mn^{2+} had been removed in the oxidative treatment.

EXAFS Spectra. EXAFS data characterizing the sample containing 1.0 wt % Mn after O_2 treatment and the best-fit model are shown in Figure 11 (the plots for the other models are shown in the Supporting Information). Each of the models that led to satisfactory fits included Mn−C, Mn−O*, and Mn−O_s contributions, described below. An attempt was made to fit the data by including an Mn−Mn contribution, but no such contribution was found (the inclusion of an Mn−Mg contribution, although it gave a model with a good fit, did not give an acceptable $(\Delta\chi)^2$ value). Details are presented in the Supporting Information. The fitting demonstrated that the data quality was less than excellent, and the *k*-range for which meaningful analysis could be done was limited to 3.08−9.50 $Å^{-1}$.

Thus, the EXAFS fits that were found to be most appropriate included Mn−C, Mn−O*, and Mn−O_s contributions (Table 2). For each of these models, the results indicate Mn−C and Mn−O* contributions with coordination numbers of approximately 3, indicating manganese tricarbonyls, consistent with the IR spectra. A Mn−O_s contribution was consistently indicated, but because of the strong correlation between the coordination number and the Debye−Waller factor, it was not possible to discriminate between the models with Mn−O_s coordination numbers of approximately 1, 2, and 3 (for models 1, 2, and 3, respectively (Table 2)). The Mn−O_s distances in each case were found to be close to 2.0 Å (Table 2). All three of these models provide satisfactory overall fits, but model 3 is preferred because the number of ligands and total valence electrons of manganese (by the 18-electron rule) is the most likely possible (see the Discussion). The lack of Mn−Mn contributions is consistent with the presence of mononuclear manganese complexes.

In summary, the data indicate that the Mn−Mn bond in $Mn_2(CO)_{10}$ had been cleaved, resulting in mononuclear manganese species, and these cationic complexes are well approximated as manganese tricarbonyls.

Discussion

Reaction of $Mn_2(CO)_{10}$ with MgO. The data clearly demonstrate that $Mn_2(CO)_{10}$ reacted with OH groups and CO_3^{2-} on the MgO surface and thus that the deposition led to some chemisorption. The IR spectra characterizing the resultant supported manganese carbonyls can be compared with the results of Keyes et al.,[29] who also used vapor deposition of $Mn_2(CO)_{10}$ to prepare MgO-supported samples. Their support was a pressed 0.3-mm-thick wafer that was thin enough for transmission IR spectroscopy; it had been pretreated at 673 K, as had our MgO. Keyes et al. observed ν_{CO} spectra as the $Mn_2(CO)_{10}$ deposition was taking place, presenting results that they interpreted as evidence of adsorption combined with breaking of Mn−Mn bonds and decarbonylation. Specifically, they observed bands at 2052, 2000, and 1978 cm^{-1} (among others), in good agreement with our bands at 2050(sh), 2000(m), and 1978(sh) cm^{-1}, for example. They inferred the presence of $Mn_2(CO)_{10}$ itself, of $[Mn(CO)_5]^-$, and of $Mn(CO)_x(O_s)_{6-x}$ (x = 2−4), in broad agreement with our data and our interpretation. However, the manganese loadings in the samples of Keyes et al. were not reported, any role of surface hydroxyl groups was overlooked, and the surface species generally consisted of complicated mixtures, in contrast to what we observed after treatment of our sample in O_2 or the samples made by adding only small amounts of $Mn_2(CO)_{10}$ to the MgO.

The oxidative fragmentation of $Mn_2(CO)_{10}$ in our work is in line with the chemistry of $Mn_2(CO)_{10}$ in solutions of nitrogen- and oxygen-donor ligands reported by Stiegman et al.[42] They observed that disproportionation and decarbonylation of $Mn_2(CO)_{10}$ occur with 1,2-bis(dimethylphosphino)ethane (dppe) or bis(2-(diphenylphosphino)ethyl)phenylphosphine (triphos), to give products including $[Mn(CO)_5]^-$ and $[Mn(CO)_xL_{6-x}]^{n+}$, where x = 0−4 and L is a ligand.

The EPR evidence of Mn^{2+} in our initially prepared sample indicates that manganese in the precursor $Mn_2(CO)_{10}$ was oxidized as a result of the chemisorption on MgO. We propose that the surface hydroxyl groups on MgO, which our IR spectra show reacted with the $Mn_2(CO)_{10}$, were the oxidizing agents. There are other examples of the oxidation of metals on oxide supports by surface hydroxyl groups, exemplified by the oxidation of ruthenium−osmium clusters on γ-Al_2O_3[43] and of rhodium clusters on γ-Al_2O_3.[44]

Oxidation of Initially Prepared Supported Manganese Carbonyls. The oxidative treatment at room temperature led to conversion of the surface manganese carbonyls, as shown by the change in the IR spectrum and by the formation of gas-phase products (such as CO) observed by mass spectrometry. The EPR data show clearly that the Mn^{2+} was removed, evidently by oxidation.

The XANES data show that the manganese was in an oxidized state after the sample had been exposed to O_2. However, as a consequence of the inconsistency in the literature regarding the XANES edge position values (Figure 10), determination of the oxidation state(s) of Mn in our sample by XANES spectroscopy is not unequivocal.

To elucidate the state of the manganese, we proceed by examining the likely forms of the manganese complexes that are expected on the basis of the known organomanganese chemistry. The most common (stable) complexes of manganese are 18-electron and 16-electron complexes.[45] We infer from the EPR data (and the treatment conditions) that the oxidation state of manganese was greater than +2. Thus, the number of bonding electrons supplied by the manganese must be less than five, with the likely value being two or four, corresponding to Mn^{5+}

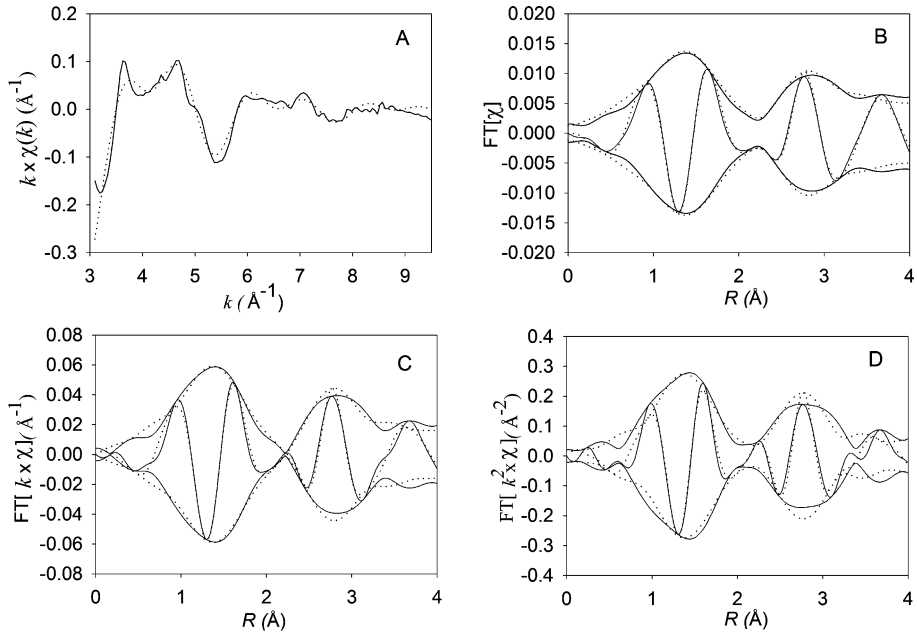

Figure 11. EXAFS data characterizing sample prepared from $Mn_2(CO)_{10}$ on MgO (1.0 wt % Mn) after O_2 treatment (—, data; •••, best fit according to model 3): k-weighted EXAFS function in k-space (A), imaginary part and magnitude of EXAFS function in R-space with FT k^0-weighting (B), FT k^1-weighting (C), and FT k^2-weighting (D).

TABLE 2: EXAFS Parameters Characterizing Sample Prepared from $Mn_2(CO)_{10}$ Supported on MgO (1.0 wt % Mn) After O_2 Treatment[a]

model no.	absorber−backscatterer pair	N	R (Å)	$\Delta\sigma^2 \times 10^{-3}$ (Å^{-2})	ΔE_0 (eV)	$(\Delta\chi)^2$ [b]
1	Mn−C	3.2	1.93	9.0	6.3	107
	Mn−O*	3.0	3.29	12.1	6.3	
	Mn−O_s	1.1	2.05	10.0	2.7	
2	Mn−C	2.7	1.92	7.8	3.9	122
	Mn−O*	3.0	3.33	11.9	3.9	
	Mn−O_s	1.8	2.00	10.5	8.9	
3	Mn−C	3.2	1.90	10.4	3.4	140
	Mn−O*	3.2	3.33	12.6	3.4	
	Mn−O_s	2.6	1.98	13.8	9.9	

[a] N, coordination number; R, distance between absorber and backscatterer atoms; $\Delta\sigma^2$, sigma-squared value (Debye−Waller factor); ΔE_0, inner potential correction; O*, oxygen of carbonyl group; O_s, oxygen atom of MgO. In the fitting, the ΔE_0 values for Mn−C and Mn−O* were constrained to be equal. Typical errors: N, ±20%; R, ±0.04 Å; $\Delta\sigma^2$, ±20%; ΔE_0, ±20%. [b] $(\Delta\chi)^2$ is a measure of the quality of the fit, as defined elsewhere.[21]

and Mn^{3+}, respectively. On the basis of the EXAFS and IR data, we are confident that the manganese complex in the oxidized sample was a manganese tricarbonyl, and we use this result in the following electron counting. The key complication is that the EXAFS data do not allow us to distinguish the Mn−O_s coordination numbers—the data are consistent with values of nearly 1, 2, and 3.

To proceed with the electron counting, we use the contradictory XANES data of Figure 10 to estimate the candidate oxidation state of the manganese. We immediately rule out the XANES data of Campos et al.[41] shown in this figure, because they indicate that the manganese in our oxidized sample was nearly Mn^{2+} contradicting our EPR data.

If, instead, the data of López et al.[39] were considered to be correct, then the comparison of our XANES result with their data would indicate that the manganese had been oxidized to Mn^{5+}. Mn^{5+} complexes are d^2 complexes, and if the tricarbonyl of Mn^{5+} were six-coordinate (the Mn−O_s coordination number would be 3, which is consistent with the EXAFS data; each oxygen of the support is regarded as a two-electron donor), then the supported manganese complex would be a 14-electron complex. Because these are rare, we discount this possibility. If the manganese tricarbonyl of Mn^{5+} were five-coordinate, it would be a 12-electron complex, which is even more unlikely and is rejected.

The remaining possibility is that the more reliable XANES standard data are those of Stueben et al.[40] According to this possibility, the manganese in the oxidized sample would be nearly Mn^{3+} (Figure 10). Mn^{3+} complexes are common; these are d^4 complexes. If the tricarbonyl of Mn^{3+} were six-coordinate (the Mn−O_s coordination number would be 3, which is consistent with the EXAFS data; again, each oxygen of the support is regarded as a two-electron donor), then the supported manganese complex would be a 16-electron complex. Because these are common, we consider this to be a highly likely possibility. Examples of six-coordinate d^4 complexes of manganese include the following:[46] $Mn(acac)_3$ (acac = acetylacetonato) and $[Mn(C_2O_4)_3]^{3-}$.

If the manganese tricarbonyl of Mn^{3+} were five-coordinate, it would be a 14-electron complex, which is highly unlikely and is rejected.

Thus, we infer that the supported manganese complex in our oxidized sample is a d^4 complex with three carbonyl ligands and bonded to MgO as a tridentate ligand. The structure is inferred to be closely comparable to one incorporating an oxometallate ligand that can be regarded as a model of an oxide surface; the corresponding compounds are $(n\text{-}Bu_4N)_2[Mn(CO)_3(H_2O)\{Mo_5O_{13}(OCH_3)_4(NO)\}]$ and $(n\text{-}Bu_4N)_3[Na\{Mo_5O_{13}(OMe)_4(NO)\}_2\{Mn(CO)_3\}_2]\cdot MeOH$,[47] which are formed by oxidation and decarbonylation of $MnBr(CO)_5$ in solution by a route that is roughly similar to ours (Me is methyl).

Correspondingly, we infer that the most likely Mn−O_s coordination number is 3 and the probable structure of our supported manganese complex is as shown in Scheme 1, where the distances are those corresponding to the preferred EXAFS model 3.

SCHEME 1: Proposed Structure of Surface Manganese Tricarbonyl Species Prepared from $Mn_2(CO)_{10}$ on MgO (1.0 wt % Mn) After O_2 Treatment[a]

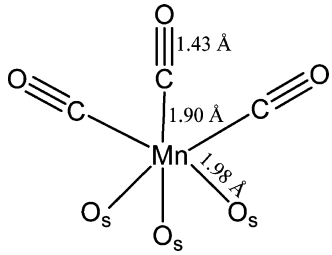

[a] The distances are in Å, as determined by EXAFS spectroscopy for the preferred model 3.

The CO stretching frequencies of the sample that is inferred to be a manganese tricarbonyl appear at lower wavenumbers than those of $Mn_2(CO)_{10}$. Although the oxidation state of manganese in the manganese tricarbonyl species (Mn^{3+}) is higher than that in $Mn_2(CO)_{10}$ (Mn^0), the presence of the three surface oxygen atoms as ligands affects the stretching frequencies of CO, which consequently shifts the CO bands to lower frequencies than those of $Mn_2(CO)_{10}$. Correspondingly, there are several examples of manganese tricarbonyl complexes with oxygen-containing ligands for which the ν_{CO} bands are at lower wavenumbers than those of $Mn_2(CO)_{10}$ (Table 1). Examples in Table 1 include complexes with strong and weak back-bonding tendencies. An example is $Mn(CO)_3(C_5H_5)Co\{P(O)R_2\}_3$,[48] which is characterized by ν_{CO} bands at 2033 and 1920 cm^{-1}. Moreover, this behavior is also observed in the rhenium tricarbonyl complexes.[49,50]

Conclusions

A sample prepared by vapor deposition of $Mn_2(CO)_{10}$ on MgO was treated in flowing O_2 at room temperature to form a species shown by IR and EXAFS spectroscopies to be a manganese tricarbonyl and shown by EPR spectroscopy to incorporate manganese in an oxidation state greater than +2. The EXAFS data and electron counting lead to the inference that the species is a d^4 complex bonded to three oxygen atoms of the MgO support as shown in Scheme 1.

Acknowledgment. S.K. is grateful for support from the program Strategic Scholarships for Frontier Research Network for the Ph.D. Program Thai Doctoral Degree from the Office of the Higher Education Commission, Thailand. This research was supported by the U.S. Department of Energy, Office of Energy Research, Basic Energy Sciences, Contract No. FG02-87ER15600. We acknowledge beam time for XAS data collection from beamline 9-BM of the Advanced Photon Source at Argonne National Laboratory. Use of the Advanced Photon Source was supported by the U.S. Department of Energy, Office of Science, Basic Energy Sciences, under Contract No. DE-AC02-06CH11357. We acknowledge the CalEPR Center at UC Davis for access to the EPR instrument.

Supporting Information Available: EXAFS spectra and Fourier transforms of EXAFS data for models 1 and 2 and the models including Mn−Mg contribution. This material is available free of charge via the Internet at http://pubs.acs.org.

References and Notes

(1) Giebeler, L.; Kiessling, D.; Wendt, G. *Chem. Eng. Technol.* **2007**, *30*, 889.
(2) Niaei, A.; Salari, D.; Aghazadeh, F.; Caylak, N.; Sepehrianazar, A. *J. Environ. Sci. Health, Part A: Toxic/Hazard. Subst. Environ. Eng.* **2010**, *45*, 454.
(3) Yang, F.; Chen, M. S.; Goodman, D. W. *J. Phys. Chem. C* **2009**, *113*, 254.
(4) Ishihara, A.; Nomura, M.; Kabe, T. *J. Catal.* **1994**, *150*, 212.
(5) Kirlin, P. S.; Knözinger, H.; Gates., B. C. *J. Phys. Chem.* **1990**, *94*, 8451.
(6) Papile, C. J.; Knözinger, H.; Gates, B. C. *Langmuir* **2000**, *16*, 5661.
(7) Yang, H. H.; Eckert, C. A. *Ind. Eng. Chem. Res.* **1988**, *27*, 2009.
(8) Vartzouma, C.; Evaggellou, E.; Sanakis, Y.; Hadjiliadis, N.; Louloudi, M. *J. Mol. Catal. A: Chem.* **2007**, *263*, 77.
(9) Zecchina, A. *J. Mol. Catal.* **1998**, *45*, 373.
(10) Burch, R.; Cruise, N.; Gleeson, D.; Tsang, S. C. *Chem. Commun.* **1996**, 951.
(11) Dossi, C.; Fusi, A.; Molteni, G.; Recchia, S.; Psaro, R. *Analyst* **1997**, *122*, 279.
(12) Paganini, M. C.; Murphy, D. M.; Ferrari, A. M.; Pacchioni, G.; Giamello, E. *J. Phys. Chem. B* **1997**, *101*, 971.
(13) Rainer, D. R.; Goodman, D. W. *J. Mol. Catal. A: Chem.* **1998**, *131*, 259.
(14) Jentoft, R. E.; Deutsch, S. E.; Gates, B. C. *Rev. Sci. Instrum.* **1996**, *67*, 2111.
(15) Koningsberger, D. C.; Mojet, B. L.; van Dorssen, G. E.; Ramaker, D. E. *Top. Catal.* **2000**, *10*, 143.
(16) Vaarkamp, M.; Linders, J. C.; Koningsberger, D. C. *Physica B* **1995**, *209*, 159.
(17) Rehr, J. J.; Albers, R. C. *Rev. Mod. Phys.* **2000**, *72*, 621.
(18) Dahl, L. F.; Rundle, R. E. *Acta Crystallogr.* **1963**, *16*, 419.
(19) Pearson, W. B.; Calvert, L. D.; Villars, P. *Pearson's Handbook of Crystallographic Data for Intermetallic Phases*; American Society for Metals: Metals Park, OH, 1985.
(20) Sayers, D. E.; Stern, E. A.; Lytle, F. W. *Phys. Rev. Lett.* **1971**, *27*, 1204.
(21) International XAFS Society, Error Reporting Recommendations: A Report of the Standard and Criteria Committee. http://ixs.iit.edu/subcommittee_reports/sc/err-rep.pdf (accessed February 2010).
(22) Ravel, B.; Newville, M. *J. Synchrotron Radiat.* **2005**, *12*, 537.
(23) Meguro, K.; Ikeya, M. *Jpn. J. Appl. Phys.* **1993**, *32*, 3540.
(24) Shpak, A. P.; Kalinichenko, E. A.; Lytovchenko, A. S.; Kalinichenko, I. A.; Legkova, G. V.; Bagmut, N. N. *Phys. Chem. Miner.* **2003**, *30*, 59.
(25) Biasia, R. S.; Grillob, M. L. N. *Solid State Commun.* **2004**, *132*, 107.
(26) Lange, J. *Phys. Rev. B: Condens. Matter Mater. Phys.* **1975**, *12*, 226.
(27) Diwald, O.; Sterrer, M.; Knözinger, E. *Phys. Chem. Chem. Phys.* **2002**, *4*, 2811.
(28) Hadjiivanov, K.; Vayssilov, G. *Adv. Catal.* **2002**, *47*, 307.
(29) Keyes, M. P.; Gron, L. U.; Watters, K. L. *Inorg. Chem.* **1989**, *28*, 1236.
(30) Bulter, I. S.; Gilson, D. F. R.; Lafleur, D. *Appl. Spectrosc.* **1992**, *46*, 1605.
(31) Yin, X.; Andersen, J. M.; Cotton, A.; Moss, J. R. *J. Organomet. Chem.* **1998**, *564*, 267.
(32) Stiegman, A. E.; Goldman, A. S.; Philbin, C. E.; Tyler, D. R. *Inorg. Chem.* **1986**, *25*, 2976.
(33) Beckett, M. A.; Brassington, D. S.; Coles, S. J.; Gelbrich, T.; Light, M. E.; Hursthouse, M. B. *J. Organomet. Chem.* **2003**, *688*, 174.
(34) Hartl, F. *Inorg. Chim. Acta* **1998**, *268*, 1.
(35) Lee, C. M.; Lin, G. Y.; Hsieh, C. H.; Hu, C. H.; Lee, G. H.; Peng, S. M.; Liaw, W. F. *J. Chem. Soc., Dalton Trans.* **1999**, 2393.
(36) Prinz, U.; Koelle, U.; Ulrich, S.; Merbach, A. E.; Maas, O.; Hegetschweiler, K. *Inorg. Chem.* **2004**, *43*, 2387.
(37) Liddle, B. J.; Wanniarachchi, S.; Lindeman, S. V.; Gardinier, J. R. *J. Organomet. Chem.* **2010**, *695*, 53.
(38) Mariscal, R.; Soria, J.; Pena, M. A.; Fierro, J. L. G. *J. Catal.* **1994**, *147*, 535.
(39) López, J. M. R.; Lede, E. J.; Requejo, F. G.; Rodriguez, J. A.; Kim, J. Y.; Salas, R. R.; Domìnguez, J. M. *J. Phys. Chem. B* **2004**, *108*, 20005.
(40) Stueben, B. L.; Cantrelle, B.; Sneddon, J.; Beck, J. N. *Microchem. J.* **2004**, *76*, 113.
(41) Campos, A.; Lohitharn, N.; Roy, A.; Lotero, E.; Goodwin, J. G.; Spivey, J. J. *Appl. Catal., A* **2010**, *375*, 12.
(42) Stiegman, A. E.; Tyler, D. R. *Inorg. Chem.* **1984**, *23*, 521.
(43) Scott, J. P.; Budge, J. R.; Rheingold, A. L.; Gates, B. C. *J. Am. Chem. Soc.* **1981**, *109*, 7736.
(44) van't Blik, H. F. J.; van Zon, J. B. A. D.; Huizinga, T.; Vis, J. C.; Koningsberger, D. C.; Prins, R. *J. Am. Chem. Soc.* **1985**, *107*, 3139.
(45) Shriver, D. F., Atkins, P. W.; Langford, C. H. *Inorganic Chemistry*; Oxford University Press: Oxford, 1990; p 503.

(46) Cotton, F. A.; Wilkinson, G. *Advanced Inorganic Chemistry: a Comprehensive Text*, 4th ed.; Wiley-Interscience: New York, 1980; p737.
(47) Villanneau, R.; Proust, A.; Robert, F.; Gouzerh, P. *Chem.—Eur. J.* **2003**, *9*, 1982.
(48) Kläui, W.; Okuda, J.; Scotti, M.; Valderrama, M. *J. Organomet. Chem.* **1985**, *280*, C26.
(49) Purnell, S. K.; Xu, X.; Goodman, D. W.; Gates, B. C. *J. Phys. Chem.* **1994**, *98*, 4076.
(50) Kirlin, P. S.; DeThomas, F. A.; Bailey, J. W.; Gold, H. S.; Dybowski, C.; Gates, B. C. *J. Phys. Chem.* **1986**, *90*, 4882.

JP104205Q